Serre–Green–Naghdi Equations with Optimized Dispersion Properties Through a Modified Auxiliary Elliptic Equation

Pierre-Henri Cocquet, Fatima-Zahra Mihami, Yann Moguen, Volker Roeber

Serre-Green-Naghdi equations with optimized dispersion properties through a modified auxiliary elliptic equation

Pierre-Henri Cocquet[a], Fatima-Zahra Mihami[b,c,*], Yann Moguen[b,d,*], Volker Roeber[b,c,**]

[a] *Université de Pau et des Pays de l'Adour, E2S UPPA, SIAME, Pau, France*
[b] *Université de Pau et des Pays de l'Adour, E2S UPPA, chaire HPC-Waves, SIAME, Anglet, France*
[c] *University of Hawai'i at Mānoa, Department of Oceanography, Honolulu, HI, USA*
[d] *Université Clermont Auvergne, Laboratoire de Mathématiques Blaise Pascal, CNRS, Clermont-Ferrand, France*

Abstract

The ability to capture frequency dispersion over a wide range is of fundamental importance for nearshore wave models that are designed for practical use in coastal engineering. Considering the Serre-Green-Naghdi equations, which are only weakly dispersive, we present and outline a strategy that can adapt the level of dispersion through a simple and easily implementable modification of the equations. The momentum equations considered as starting point contain an elliptic equation, which determines the non-hydrostatic pressure. The proposed modified system is designed in a way to facilitate the optimization of its dispersion properties through a finite difference discretization of the linearized equations. Due to the fact that the improvement of the dispersion properties is performed through modification of the elliptic part of the governing equations, the introduced term for improving the dispersion properties is of order σ^4 according to Airy wave theory, where σ is the shallowness parameter. This differs from classical methods for dispersion improvement and is of advantage for both numerical and theoretical reasons. Although the presented justification is based on a linear dispersion analysis assuming zero bathymetry variation, numerical comparison with experimental data shows that the modified system provides encouraging results even over a spatially varying bottom.

Keywords: Serre-Green-Naghdi equations, Dispersion, Depth-integrated models, Non-hydrostatic models.

1. Introduction

On most beaches, swell waves are the controlling factor for the overall shape of the beach and the durability and effectiveness of coastal protection structures. With an increasing use of phase-resolving nearshore wave models for practical use in coastal engineering, their ability to accurately capture frequency dispersion of short waves is of fundamental importance; see *e.g.*[1, 2, 3, 4].

Various flow models are used in coastal engineering and applied geophysics. Their grouping into families regarding non-linearity and non-hydrostasy, which is the origin of dispersion effects, is based on the introduction of dimensionless numbers, including the shallowness parameter:

$$\sigma = \frac{b_0}{\lambda_0},$$

where b_0 is a typical water depth and λ_0 is a typical horizontal wavelength; and the amplitude parameter:

$$\epsilon = \frac{\eta_0}{b_0},$$

where η_0 is a typical wave amplitude. The approximate flow models used for nearshore waves, where it is desirable to take dispersion into account, are derived from the free surface Euler equations for non-viscous fluid, or, if irrotationality is assumed, from the Laplace equation (see *e.g.*[5, 6, 7]). The first step of derivation

*present address
**Corresponding author
Email address: volker.roeber@univ-pau.fr (Volker Roeber)

is a depth-integration of the basic equations. Then, one usually distinguishes between weakly dispersive and weakly non-linear Boussinesq equations, for which $O(\sigma^2)$-terms are kept and with ϵ belonging to $O(\sigma^2)$, and the Serre-Green-Naghdi equations [8, 9, 10], which are fully non-linear (no assumption on ϵ) but also weakly dispersive. Note that it is possible to derive Boussinesq-type models with dispersion properties higher than those of the basic Boussinesq equations (see *e.g.* [11, 12]), but in the present study we focus on the dispersion improvement of the Serre-Green-Naghdi equations.

The basic ideas for improving the dispersion properties of the Serre-Green-Naghdi equations originate from the work by Witting [13] (see also Schröter *et al.* [14] in the same vein), where the analysis was carried out in the case of a flat bottom, and the (Padé) approximation of the dispersion relation is for linear waves. This strategy was used by many authors (*e.g.* by Madsen *et al.* [15]; see below for other examples): the correction constructed in this way is used, sometimes after adaptation, in cases where the bathymetry varies (see *e.g.* Madsen and Sørensen [16]). Considering also the case of a constant bathymetry, we can roughly distinguish three families of methods to improve the dispersion properties of the Serre-Green-Naghdi equations:

The first family of methods originates from the work by Madsen *et al.* [15] (see also, *e.g.*, [17, 18]). Considering the 1-D (horizontal) equations to simplify the presentation, it consists in adding the terms

$$\alpha b^2 \left[\partial_{xxt} v + \partial_{xx}(v\partial_x v) + g\partial_{xxx} h\right]$$

to the right-hand side of the momentum equation, which can be written as

$$\partial_t v + v\partial_x v + g\partial_x \eta = \frac{1}{h}\partial_x \widetilde{p},$$

with h the water depth, η the surface elevation, b the bathymetry, v the depth-averaged horizontal velocity, g the acceleration of gravity, $\widetilde{p}$ the non-hydrostatic pressure and α the parameter to be optimized for the improvement of dispersion. As it can be considered that $\partial_x(\cdot)$ and $\partial_t(\cdot)$ belong to $O(\sigma)$, the added term, that is equal to $\alpha b^2 \partial_{xx}\left(h^{-1}\partial_x \widetilde{p}\right)$ where $\widetilde{p}$ is $O(\sigma^2)$ (this can be seen directly from Equations (4) and (5) in Section 2), belongs to $O(\sigma^5)$.

The second family of methods, first proposed by Liu and Sun [19] (see also [20, 21] and the discussion in [22]), can be explained as follows. From the momentum equation above, we have

$$-\frac{3}{h^2}\widetilde{p} = 2h(\partial_x v)^2 + gh\partial_{xx} h - h\partial_x\left(\frac{1}{h}\partial_x \widetilde{p}\right),$$

so that

$$\widetilde{p} = \widetilde{p}^{\,\mathrm{approx}} + O(\sigma^4), \quad \text{with} \quad \widetilde{p}^{\,\mathrm{approx}} = -\frac{h^3}{3}[2(\partial_x v)^2 + g\partial_{xx} h].$$

Then, averaging by $(1-\beta)$ and β the exact and the approximate expressions of $\widetilde{p}$, the momentum equation to be solved becomes

$$\partial_t v + v\partial_x v + g\partial_x \eta = \frac{1}{h}\partial_x \widetilde{p}_\beta, \quad \text{where} \quad \widetilde{p}_\beta = \beta\widetilde{p}^{\,\mathrm{approx}} + (1-\beta)\widetilde{p}. \tag{1}$$

Thus,

$$\widetilde{p}_\beta = (1-\beta)\widetilde{p} + O(\beta\sigma^2),$$

so that, for a fixed β, the dispersion properties of the Serre-Green-Naghdi equations are modified by adding a $O(\sigma^3)$-term to the momentum equation.

A third family is the method proposed by Bonneton *et al.* [23] and Chazel *et al.* [24] (see also [25]). It relies on a formulation of the momentum equation, initially proposed in [26], as

$$(\mathcal{I} + \mathcal{L})(\partial_t v + v\partial_x v) + \partial_x \eta + \mathcal{Q}(v) = 0,$$

where $\mathcal{L}$ and $\mathcal{Q}$ are a linear differential operator and a quadratic form, respectively. The parameter α is introduced through an averaging similar to that used for the derivation of the second-family method but applied here on the term $\partial_t v$. This results in

$$(\mathcal{I} + \alpha\mathcal{L})(\partial_t v + v\partial_x v) + [\mathcal{I} - (1-\alpha)\mathcal{L}]\partial_x \eta + \mathcal{Q}(v) = 0.$$

It is of particular interest regarding the present study to note that a variant with solution of mass and momentum equations coupled to an auxiliary elliptic equation was proposed by Chassagne *et al.* [27] (see also [28]). For improvement of dispersion, the momentum equation is not modified and the parameter α is inserted into the elliptic equation as

$$\partial_x \widetilde{p} + \alpha \mathcal{L}(\partial_x \widetilde{p}) = \mathcal{L}(gh\partial_x \eta) - \mathcal{Q}(v),$$

where $\mathcal{L}(\phi) = -\partial_x \left[h^3 \partial_x (h^{-1}\phi)\right]$ and $\mathcal{Q}(v) = 2\partial_x \left[h^3 (\partial_x v)^2\right]/3$. An obvious advantage that can be first noted from the resulting three-equation model, namely with the elliptic equation coupled to the mass and momentum equations, is that it is simple to implement, since no new terms with derivatives need to be added to the equations of the original model. A second obvious advantage is that the dispersion correction thus performed does not require the addition of terms with high-order derivatives in dispersion correction terms, which often compromise numerical stability; see Cienfuegos *et al.* [18]. We also see that the term added to improve the dispersion properties of the system belongs to $O(\sigma^4)$, which can be of interest compared to the $O(\sigma^5)$-terms added in the first family of methods - with the potential numerical issues mentioned previously - and compared to the second family of methods with $O(\sigma^3)$-terms added to the momentum equation, hence of the same order as dispersive terms present in the original equation. It is this approach that we outline in detail in the present study, following the three-equation formulation with the auxiliary elliptic equation in the form proposed by Khakimzyanov *et al.* [29].

The layout of the paper is the following. In Section 2 we recall the different forms of the Serre-Green-Naghdi equations, including when an auxiliary elliptic equation is present. Section 3 is devoted to the derivation and justification of a dispersion correction based on an elliptic equation. In particular, the relationship, when the dispersion correction parameter is small, between the linear system used to derive the method and the non-linear system to which it is applied, is examined. A straightforward numerical method allowing momentum conservation on a staggered grid, and a set of tests are finally presented in Section 4.

2. Different forms of the Serre-Green-Naghdi equations

The Serre-Green-Naghdi (SGN) equations are first given with space-varying bathymetry, since bathymetry terms are taken into account in some tests presented at the end of this study. With the momentum equation in non-conservative form, as it is often found, the one-dimensional SGN equations, are (see *e.g.* [30, 18, 29, 31])

$$\partial_t h + \partial_x (hv) = 0, \tag{2}$$

$$\partial_t v + v\partial_x v + g\partial_x \eta = \frac{1}{h}\left(\partial_x \widetilde{p} - p_b \partial_x b\right), \tag{3}$$

where h is the water depth, v is the depth-averaged horizontal velocity, b is the bathymetry or water depth at rest, $\eta = h - b$ is the surface elevation and g is the acceleration of gravity. Moreover, $\widetilde{p}$ is the depth-integrated non-hydrostatic pressure defined as

$$\widetilde{p} = -\frac{h^2}{3}\left(\gamma_s + \frac{1}{2}\gamma_b\right), \tag{4}$$

with

$$\gamma_b = -v^2 \partial_{xx} b - \left(\partial_t v + v\partial_x v\right)\partial_x b, \qquad \gamma_s = \gamma_b + h\left[(\partial_x v)^2 - \partial_{xt} v - v\partial_{xx} v\right], \tag{5}$$

which are approximations of the vertical accelerations of the water column at the bottom and at the free surface, respectively (see *e.g.* [32, 18]), and p_b is the non-hydrostatic pressure at the bottom, defined as

$$p_b = -\frac{h}{2}\left(\gamma_s + \gamma_b\right).$$

Using the continuity equation (2) and the momentum equation in non-conservative form, (3), the momentum balance can be written in conservative form as

$$\partial_t (hv) + \partial_x (hv^2 + p) = \partial_x \widetilde{p} + (gh - p_b)\partial_x b, \tag{6}$$

where $p = gh^2/2$ is the depth-integrated hydrostatic pressure. Equations (2) and (6) result in the SGN model in conservative form. Also, following Khakimzyanov *et al.* [29], it can be observed that the depth-integrated non-hydrostatic pressure $\widetilde{p}$ satisfies the elliptic equation

$$\partial_x\left(\frac{\partial_x\widetilde{p}}{h}\right) - \frac{3}{h^3}\widetilde{p} = g\partial_{xx}\eta + 2(\partial_x v)^2 + \partial_x\left(\frac{p_b}{h}\partial_x b\right) + \frac{3}{2h}\gamma_b, \tag{7}$$

obtained from Equations (3), (4) and (5). Equation (7) can be solved coupled to Equations (2) and (3), or (2) and (6), the whole sets forming another form of the SGN equations. Indeed, exploiting the relation

$$p_b = \frac{3}{2h}\widetilde{p} - \frac{h}{4}\gamma_b,$$

Equation (7) can be recast as

$$4\partial_x\left(\frac{\partial_x\widetilde{p}}{hY}\right) - 6\left[\frac{2}{h^3}\,\frac{Y-3}{Y} + \partial_x\left(\frac{\partial_x b}{h^2 Y}\right)\right]\widetilde{p} = \partial_x\left(g\partial_x\eta + \frac{R\partial_x b}{Y}\right) - 6\frac{R}{hY} + 2\left(\partial_x v\right)^2, \tag{8}$$

where $Y = 4 + (\partial_x b)^2$ and $R = -g\partial_x\eta\partial_x b + v^2\partial_{xx}b$. It is with this latter form of the elliptic equation that Khakimzyanov *et al.* propose to numerically solve the SGN equations. We follow this approach in the present study and we will use Equation (8) to define the proposed modification of the SGN equations.

3. Modified Serre-Green-Naghdi equations and their dispersion properties

The original SGN system considered in this paper is given by Equations (2),(3) together with the elliptic equation (8). The dispersion correction we propose is based on a modification of the elliptic equation (8) and the modified SGN system is defined as

$$\begin{cases} \partial_t h + \partial_x(hv) = 0, \\ \partial_t v + v\partial_x v + g\partial_x\eta = \dfrac{1}{h}\left(\partial_x\widetilde{p} - p_b\partial_x b\right), \\ 4(1+\delta)\partial_x\left(\dfrac{\partial_x\widetilde{p}}{hY}\right) - 6\left[\dfrac{2}{h^3}\,\dfrac{Y-3}{Y} + \partial_x\left(\dfrac{\partial_x b}{h^2 Y}\right)\right]\widetilde{p} = \partial_x\left(g\partial_x\eta + \dfrac{R\partial_x b}{Y}\right) - 6\dfrac{R}{hY} + 2\left(\partial_x v\right)^2. \end{cases} \tag{9}$$

We emphasize that we recover the original SGN equations, namely (2)-(3)-(8), when $\delta = 0$. Note that the $\partial_x\widetilde{p}$-term of the momentum equation belongs to $O(\sigma^3)$ only, so introducing the factor $(1+\delta)$ in this term would modify the SGN system at the order of σ^3. Instead, we use the elliptic equation fulfilled by the non-hydrostatic $\widetilde{p}$ to modify the dispersion of the SGN model. In the elliptic equation of the set (9), the term modified by the factor $(1+\delta)$ belongs to $O(\sigma^4)$, which allows to gain one order of magnitude as $\sigma \to 0$.

3.1. Interpretation of the modified Serre-Green-Naghdi equations for small parameter δ

In this Section, some additional information related to the modified SGN equations for small δ are given.

As here the bathymetry is assumed to be constant, the modified SGN system with elliptic equation (7) - which is equivalent to the form (9) -, is

$$\begin{cases} \partial_t h + \partial_x(hv) = 0, \\ \partial_t v + v\partial_x v + g\partial_x h = \dfrac{1}{h}\partial_x\widetilde{p_\delta}, \\ (1+\delta)\partial_x\left(\dfrac{\partial_x\widetilde{p_\delta}}{h}\right) - \dfrac{3}{h^3}\widetilde{p_\delta} = g\partial_{xx}h + 2(\partial_x v)^2. \end{cases} \tag{10}$$

Taking the derivative with respect to x of the second equation and inserting the obtained expression into the elliptic equation results in

$$\delta\partial_x\left(\frac{\partial_x\widetilde{p_\delta}}{h}\right) - \frac{3}{h^3}\widetilde{p_\delta} = (\partial_x v)^2 - \partial_{xt}v - v\partial_{xx}v = \frac{\gamma_s}{h}. \tag{11}$$

For $\delta = 0$, Equation (11) directly gives the depth-integrated non-hydrostatic pressure $\widetilde{p}$ as a function of h and v. This shows once again that, for $\delta = 0$, one can get $\widetilde{p}$ without solving the elliptic equation. The latter facilitates the numerical calculations (see the discussion in the Introduction Section and Section 4.1). However, when $\delta \neq 0$, it is evident from Equation (11) that h, v and $\widetilde{p}_\delta$ satisfy a fully coupled non-linear system, for which $\widetilde{p}_\delta$ is no longer the depth-integrated non-hydrostatic pressure as defined by Equation (4). To explain further how the solution of Equations (10) is related to the one of the original SGN systems, we now present an analysis as $\delta \to 0$.

Assuming δ to be small, we postulate the expansions

$$h = h_0 + h_1\delta + \cdots, \; v = v_0 + v_1\delta + \cdots, \; \widetilde{p_\delta} = \widetilde{p}_0 + \widetilde{p}_1\delta + \cdots.$$

Inserting these into the modified SGN equations, we find that h_0, v_0 and $\widetilde{p}_0$ satisfy the original (namely with $\delta = 0$) SGN system. In addition, Equation (11) gives

$$-\frac{3}{h_0^3}\widetilde{p}_0 = \frac{\gamma_{0,s}}{h_0}, \quad \text{with } \gamma_{0,s} = h_0\left[(\partial_x v_0)^2 - \partial_{xt}v_0 - v_0\partial_{xx}v_0\right].$$

As expected, the zeroth-order term of the non-hydrostatic pressure expansion is exactly the non-hydrostatic pressure defined by Equation (4):

$$\widetilde{p}_0 = -\frac{h_0^2}{3}\gamma_{0,s}.$$

Continuing the identification, the first-order perturbations are solutions to

$$\begin{aligned}
&\partial_t h_1 + \partial_x(h_0 v_1 + h_1 v_0) = 0,\\
&\partial_t v_1 + v_0\partial_x v_1 + v_1\partial_x v_0 + g\partial_x h_1 = \frac{1}{h_0}\partial_x\widetilde{p_1} - \frac{h_1}{h_0^2}\partial_x\widetilde{p_0}.
\end{aligned}$$

The first-order perturbation of the depth-integrated non-hydrostatic pressure, $\widetilde{p}_1$, can be obtained from Equation (11) by

$$-\frac{3}{h_0^3}\widetilde{p_1} = -9\frac{h_1}{h_0^4}\widetilde{p_0} + (2\partial_x v_0\partial_x v_1 - \partial_{xt}v_1 - v_0\partial_{xx}v_1 - v_1\partial_{xx}v_0) - \partial_x\left(\frac{\partial_x\widetilde{p_0}}{h_0}\right).$$

As $\widetilde{p_0}$ satisfies the elliptic equation associated with the original SGN system, we obtain

$$\widetilde{p_1} = \left(1 + 3\frac{h_1}{h_0}\right)\widetilde{p}_0 - \frac{h_0^3}{3}\left[2\partial_x v_0\partial_x v_1 - \partial_{xt}v_1 - v_0\partial_{xx}v_1 - v_1\partial_{xx}v_0 - g\partial_{xx}h_0 - 2(\partial_x v_0)^2\right]. \quad (12)$$

The first-order perturbation of the depth-integrated non-hydrostatic pressure is thus determined.

We now study how to eliminate the modified elliptic equation, and thus rewrite the modified SGN system as a set of two equations for the water depth and the depth-averaged horizontal velocity. Assuming that the first-order perturbations of h and v vanish and dropping the subscript 0 to work with h and v, the modified non-hydrostatic pressure $\tilde{p}_\delta = \tilde{p}_0 + \delta\tilde{p}_1$ given by Equation (12) then reduces to

$$\widetilde{p_\delta} = -\frac{h^2}{3}\gamma_s + \delta\left\{-\frac{h^2}{3}\gamma_s + \frac{h^3}{3}\left[g\partial_{xx}h + 2(\partial_x v)^2\right]\right\}. \quad (13)$$

Inserting this expression into Equations (10), the modified SGN equations can be rewritten as the following two-equation set:

$$\begin{cases}
\partial_t h + \partial_x(hv) = 0,\\
\partial_t v + v\partial_x v + g\partial_x h = \dfrac{1}{h}\partial_x\left(-(1+\delta)\dfrac{h^2}{3}\gamma_s + \delta\left\{\dfrac{h^3}{3}\left[g\partial_{xx}h + 2(\partial_x v)^2\right]\right\}\right).
\end{cases} \quad (14)$$

Now, $\widetilde{p}_\delta$ given by Equation (13) where h and v satisfy Equations (14), is a solution up to $O(\delta^2)$ of the modified elliptic equation obtained from Equation (10).

Remark 1: *The linearization of the two-equation form* (14) *of the modified SGN system gives*

$$\left\{\begin{array}{l} \partial_t \eta + b\partial_x v = 0, \\ \partial_t v + g\partial_x \eta = (1+\delta)\dfrac{b^2}{3}\partial_{xxt} v + g\delta\dfrac{b^2}{3}\partial_{xxx}\eta. \end{array}\right. \tag{15}$$

Equations (15) *are the same as [22, Eqs. (51)-(52)] with* $\beta = 3\delta/2$ *and the same as the linearized model from [19] (see also* (1)*). However, returning to the non-linear equations, the two-equation form* (14) *is different from the consistent modification of the Serre equations from [22, Eqs. (36)-(38)], whose momentum equation is*

$$\partial_t v + v\partial_x v + g\partial_x h = \frac{1}{h}\partial_x\left\{-(1+\delta)\frac{h^2}{3}\gamma_s + \delta\left[g\frac{h^3}{3}\partial_{xx}h + gh^2\frac{(\partial_x h)^2}{2}\right]\right\}. \tag{16}$$

The difference between the two momentum equations (14) *and* (16) *lies in the right-hand sides, where the term* $2h^3(\partial_x v)^2/3$ *in* (14) *is replaced by* $gh^2(\partial_x h)^2/2$ *in* (16)*. Nevertheless, setting* $\beta = -\delta$ *in* (1) *which is derived from [19], we see that* $\widetilde{p}_\beta = \widetilde{p}_\delta$ *where* $\widetilde{p}_\delta$ *is given by* (13)*. As a result,* (1) *is exactly the two-equation form* (14) *of the modified SGN system we propose.*

3.2. Phase velocity associated to the modified Serre-Green-Naghdi equations

With $h = b + \eta$, where b is the constant bathymetry, the linearization of the modified SGN equations (9) (see also Equations (10)) results in

$$\left\{\begin{array}{l} \partial_t \eta + b\partial_x v = 0, \\ \partial_t v + g\partial_x \eta = \dfrac{1}{b}\partial_x \tilde{p}, \\ (1+\delta)\partial_{xx}\tilde{p} - \dfrac{3}{b^2}\tilde{p} = gb\partial_{xx}\eta, \end{array}\right. \tag{17}$$

where $\delta > 0$ is going to be optimized to have the wave velocity associated to the modified SGN equations (9) as close as possible to the wave velocity of the Airy theory. It can be noted that the linearization of the original SGN equations is obtained from Equations (17) by setting $\delta = 0$.

The phase velocity associated to Equations (17) are obtained by considering the plane wave solutions $\boldsymbol{X}\mathrm{e}^{\mathrm{i}(kx-\omega t)}$. Now, non-zero solutions of

$$\boldsymbol{A}(\omega,k)\boldsymbol{X} = \boldsymbol{0}, \quad \text{where } \boldsymbol{A}(\omega,k) = \begin{bmatrix} -\mathrm{i}\omega & -\mathrm{i}bk & 0 \\ -\mathrm{i}gk & -\mathrm{i}\omega & \mathrm{i}\dfrac{k}{b} \\ gbk^2 & 0 & -(1+\delta)k^2 - \dfrac{3}{b^2} \end{bmatrix},$$

are obtained if

$$b^3gk^4\delta - b^2k^2\delta w^2 - b^2k^2\omega^2 + 3bgk^2 - 3\omega^2 = 0.$$

The phase velocity of the modified SGN equations is thus

$$c_{\mathrm{SGN},\delta}(kb) = \frac{\omega}{k} = \sqrt{gb}\sqrt{\frac{1+(kb)^2\delta/3}{1+(1+\delta)(kb)^2/3}}.$$

As the phase velocity of the original SGN equations is retrieved for $\delta = 0$, we set

$$c_{\mathrm{SGN}}(kb) = c_{\mathrm{SGN},0}(kb) = \sqrt{gb}\sqrt{\frac{1}{1+(kb)^2/3}}.$$

In addition, a Taylor expansion as $\delta \to 0$ gives

$$c_{\mathrm{SGN},\delta}(kb) - c_{\mathrm{SGN}}(kb) = \delta\int_0^1 \partial_\delta c_{\mathrm{SGN},t\delta}(kb)\,\mathrm{d}t, \tag{18}$$

where

$$\partial_\delta c_{\mathrm{SGN},s}(kb) = \frac{\sqrt{gb}}{2} \frac{(kb)^4}{[(1+s)(kb)^2+3]^{3/2}\sqrt{s(kb)^2+3}}$$

is the derivative of c_{SGN} with respect to δ. Since $c_{\mathrm{SGN}}(0) = c_{\mathrm{SGN},0}(0)$ for any δ, it can be assumed that $kb > 0$. Then,

$$\begin{aligned} \left| \int_0^1 \partial_\delta c_{\mathrm{SGN},t\delta}(kb)\,\mathrm{d}t \right| &\leq \int_0^1 \frac{\sqrt{gb}}{2} \frac{(kb)^4}{[(1+t\delta)(kb)^2]^{3/2}\sqrt{3}}\,\mathrm{d}t \\ &= \sqrt{gb}\frac{kb}{2\sqrt{3}} \int_0^1 \frac{1}{(1+t\delta)^{3/2}}\,dt \leq \sqrt{gb}\frac{kb}{2\sqrt{3}}. \end{aligned}$$

With Equation (18),

$$c_{\mathrm{SGN},\delta}(kb) = c_{\mathrm{SGN}}(kb) + O(\delta\, kb). \tag{19}$$

Thus, if $kb \leq M$ for some $M > 0$, and if δ is small enough, the dispersion properties of the modified SGN equations are close to those of the original SGN equations up to order δ.

Remark 2: *Assuming that $kb > 0$,*

$$\begin{aligned} \left| \int_0^1 \partial_\delta c_{\mathrm{SGN},t\delta}(kb)\,\mathrm{d}t \right| &\leq \frac{1}{2\sqrt{\delta}} \int_0^1 \frac{(kb)^4}{[(1+t\delta)(kb)^2]^{3/2}\sqrt{t\,(kb)^2}}\,\mathrm{d}t \\ &\leq \frac{\sqrt{gb}}{2\sqrt{\delta}} \int_0^1 \frac{1}{(1+t\delta)^{3/2}\sqrt{t}}\,\mathrm{d}t \\ &\leq \frac{\sqrt{gb}}{2\sqrt{\delta}} \int_0^1 \frac{1}{\sqrt{t}}\,\mathrm{d}t = \frac{\sqrt{gb}}{\sqrt{\delta}}, \end{aligned}$$

and thus, with Equation (18)*,*

$$\sup_{kb\geq 0} |c_{\mathrm{SGN},\delta}(kb) - c_{\mathrm{SGN}}(kb)| = O\left(\sqrt{\delta}\right).$$

Comparing this result with Equation (19)*, the dependence in kb has disappeared, but at the cost of a decrease in the order of accuracy. In the following, kb will be considered such that $kb \leq M$, and thus the modified SGN equations approximate the phase velocity of the original SGN equations up to $O(\delta)$. This is consistent with the fact that the modified SGN set of equations is a regular perturbation of the SGN equations.*

We now seek for $\delta_{\min}$ such that $c_{\mathrm{SGN},\delta}$ is as close as possible to c_{Airy} given by

$$c_{\mathrm{Airy}}(kb) = \sqrt{gb}\sqrt{\frac{\tanh(kb)}{kb}}.$$

Setting $x = kb$,

$$J(\delta) = \left\{ \frac{1}{x_{\max}} \int_0^{x_{\max}} \left[c_{\mathrm{SGN},\delta}(x) - c_{\mathrm{Airy}}(x)\right]^2\,\mathrm{d}x \right\}^{1/2},$$

is discretized using a uniform subdivision with N points of the interval $[0, x_{\max}]$, and then minimized using the Nelder-Mead algorithm with $\delta = 0$ as initial guess.

In Figure (1) are shown some results for varying $x_{\max}$ and in Table 1 are given values of J before and after optimization as well as $\delta_{\min}$. From this results, it is observed that, as $x_{\max}$ increases, $\delta_{\min}$ decreases but $J(\delta_{\min})$ increases. In Figure 2 is evidenced the dependence on $x_{\max}$ of $\delta_{\min}$ and $J(\delta_{\min})$. It is shown in Figure 2 that $\delta_{\min} \approx 0.2$ for small values of $x = kb$ and that, for large values of kb, $\delta_{\min}$ has a finite limit value.

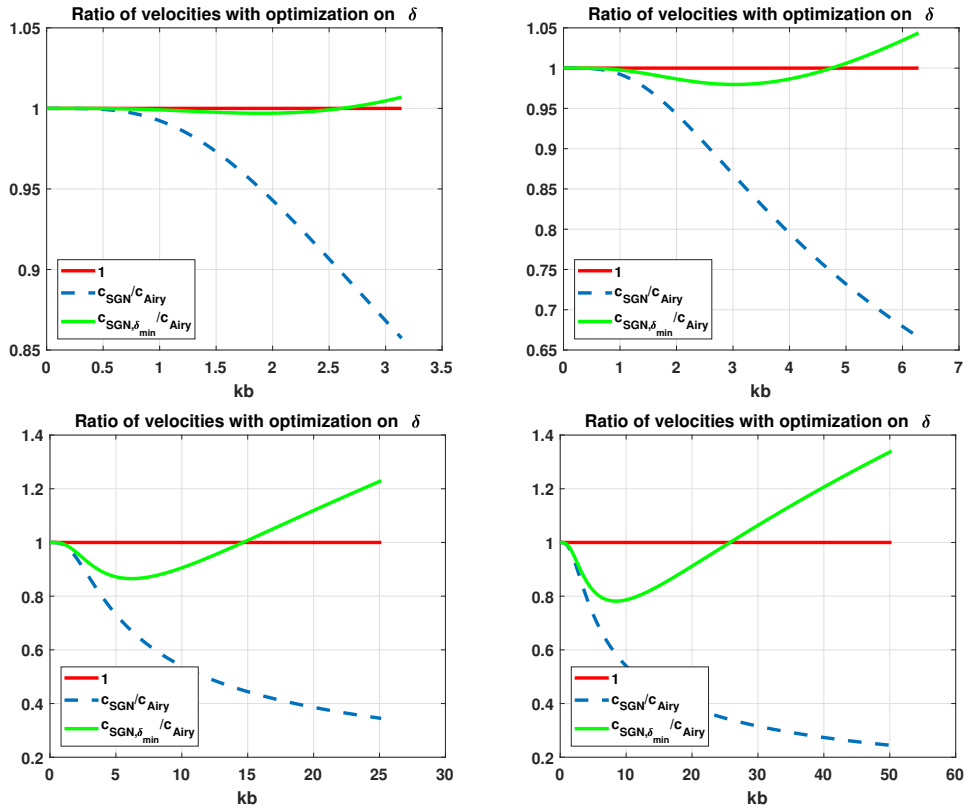

Figure 1: $c_{\mathrm{SGN},\delta_{\min}}/c_{\mathrm{Airy}}$ for several values of $x_{\max}$. Up left: $x_{\max}=\pi$, up right: $x_{\max}=2\pi$, bottom left: $x_{\max}=4\pi$, bottom right: $x_{\max}=8\pi$. $N=100$.

$x_{\max}$	$J(0)$	$J(\delta_{\min})$	$\delta_{\min}$
π	0.12504	0.0046825	0.17
2π	0.26704	0.02584	0.13375
4π	0.36867	0.065371	0.092875
8π	0.40214	0.10452	0.059313
16π	0.38512	0.12945	0.035875

Table 1: Value of J and $\delta_{\min}$ for various $x_{\max}$. $N=100$.

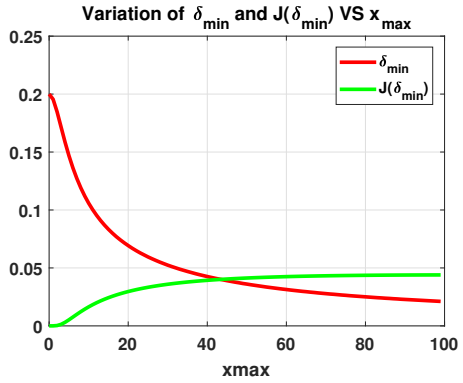

Figure 2: $\delta_{\min}$ and $J(\delta_{\min})$ for varying $x_{\max}$.

3.2.1. Optimized δ-parameter for small reduced wavenumber kb

In this Subsection, we compute the optimal value of δ for which the phase velocity associated with the modified SGN equations matches the Airy velocity when kb goes to zero. This derivation is done by matching the Taylor expansions of both phase velocities as $kb \to 0$.

Since

$$c_{\mathrm{SGN},\delta}(kb) = \sqrt{gb}\left[1 - \frac{1}{6}(kb)^2 + \left(\frac{\delta}{18} + \frac{1}{24}\right)(kb)^4\right] + O((kb)^6),$$

and

$$c_{\mathrm{Airy}}(kb) = \sqrt{gb}\left[1 - \frac{1}{6}(kb)^2 + \frac{19}{360}(kb)^4\right] + O((kb)^6),$$

we can have $c_{\mathrm{SGN},\delta}$ close to c_{Airy} for small kb if δ satisfies

$$\frac{\delta}{18} + \frac{1}{24} = \frac{19}{360}.$$

Then, for $\delta = 1/5$,

$$c_{\mathrm{SGN},\delta}(kb) - c_{\mathrm{Airy}}(kb) = O((kb)^6),$$

instead of being $O((kb)^4)$. This confirms what what can be seen in Figure 2, *i.e.* that the optimal value of δ for kb small enough is $\delta = 1/5$.

3.2.2. Matching phase velocities for a given value of reduced wavenumber kb

The optimization results from the previous Subsection are very useful for problems involving several spatial frequencies. For one fixed frequency $kb = x_0$, we can look for δ_0 such that

$$c_{\mathrm{SGN},\delta_0}(x_0) = c_{\mathrm{Airy}}(x_0).$$

The previous equation can be solved exactly and gives

$$\delta_0 = \frac{x_0^2\exp(2x_0) - 3x_0\exp(2x_0) - x_0^2 + 3\exp(2x_0) - 3x_0 - 3}{[x_0\exp(2x_0) - \exp(2x_0) + x_0 + 1]x_0^2}. \tag{20}$$

This is the value of δ for which, for fixed kb, the phase velocity of the modified SGN matches the Airy wave theory. It is worth noting that, as $x_0 \to 0$,

$$\delta_0 = \frac{1}{5} + O(x_0).$$

The optimal value $\delta_{\min} = 1/5$ for small enough kb is thus again recovered.

Remark 3: Comparison with dispersion properties of Nwogu equations
The wave velocity associated to Nwogu equations [33] is

$$c_{\mathrm{Nwogu}}(kb) = \sqrt{gb}\sqrt{\frac{1 - (\alpha + 1/3)(kb)^2}{1 - \alpha(kb)^2}}.$$

Let us recall that the wave velocity of the modified SGN system is

$$c_{\mathrm{SGN},\delta}(kb) = \sqrt{gb}\sqrt{\frac{1 + b^2k^2\delta/3}{1 + (1+\delta)b^2k^2/3}}.$$

If $\delta = -3\alpha - 1$, then $\delta/3 = -(\alpha + 1/3)$ and $(1+\delta)/3 = -\alpha$, and thus

$$c_{\mathrm{SGN},\delta}(kb) = c_{\mathrm{Nwogu}}(kb).$$

The proposed modified SGN system thus has the same dispersion properties as the Nwogu system.

$x_{\max}$	$J_g(0)$	$J_g(\delta_{\min,g})$	$J_g(\delta_{\min})$	$\delta_{\min,g}$
π	0.1022	0.0073	0.0108	0.1549
2π	0.1498	0.0286	0.0398	0.1054
4π	0.1538	0.0511	0.0697	0.0609
8π	0.1362	0.0613	0.0832	0.0324
16π	0.1126	0.0604	0.0822	0.0167

Table 2: Value of J_g and $\delta_{\min,g}$ for various $x_{\max}$. $N = 100$. The value of $\delta_{\min}$ is the one minimizing J from Table 1.

3.3. Group velocity

We now investigate the group velocity of the modified SGN system. It is defined as

$$c_g = \partial_k \omega = \partial_k (kc) = k\partial_k c + c,$$

so that for the Airy wave theory,

$$c_{g,\mathrm{Airy}}(kb) = \frac{\sqrt{gb}}{2} \frac{\sinh(kb)\cosh(kb) + kb}{[\cosh(kb)]^{3/2}\sqrt{kb\sinh(kb)}},$$

and for the modified SGN system,

$$c_{g,\mathrm{SGN},\delta} = \sqrt{gb}\frac{(kb)^4\delta^2 + (kb)^4\delta + 6(kb)^2\delta + 9}{[(kb)^2\delta + (kb)^2 + 3]^{3/2}\sqrt{\delta(kb)^2 + 3}}.$$

For the original SGN system, $c_{g,\mathrm{SGN}} = c_{g,\mathrm{SGN},0}$. Taylor expansions for $kb \to 0$ give

$$\begin{aligned}
c_{g,\mathrm{Airy}} &= \sqrt{gb}\left[1 - \frac{1}{2}(kb)^2 + \frac{19}{72}(kb)^4\right] + O((kb)^6),\\
c_{g,\mathrm{SGN},\delta} &= \sqrt{gb}\left[1 - \frac{1}{2}(kb)^2 + \left(\frac{5}{18}\delta + \frac{5}{24}\right)(kb)^4\right] + O((kb)^6),
\end{aligned}$$

which show that the group velocity associated to the original SGN equations (with $\delta = 0$) approximates the one of the Airy theory up to $O((kb)^4)$. Choosing δ such that

$$\frac{5}{18}\delta + \frac{5}{24} = \frac{19}{72},$$

which yields $\delta = 1/5$, we obtain that the group velocity of the modified SGN equations approximates the group velocity of the Airy wave theory up to $O((kb)^6)$ instead of $O((kb)^4)$.

We now compute $\delta_{\min,g}$ that minimizes

$$J_g(\delta) = \left\{\frac{1}{x_{\max}}\int_0^{x_{\max}} \left[c_{g,\mathrm{SGN},\delta}(x) - c_{g,\mathrm{Airy}}(x)\right]^2 \,\mathrm{d}x\right\}^{1/2}.$$

Again, a uniform subdivision of $[0, x_{\max}]$ with N points is used, and the previous function is minimized using the Nelder-Mead algorithm with $\delta = 0$ as an initial guess. The results are shown in Figure 3 for the ratio of group velocities and in Table 2 for some numerical values. We compare what happened when using either $\delta_{\min}$ (the value minimizing phase dispersion error) or $\delta_{\min,g}$ which minimizes the gap between group velocities. It is worth noting that a minimization of the phase error still reduces the group velocity error.

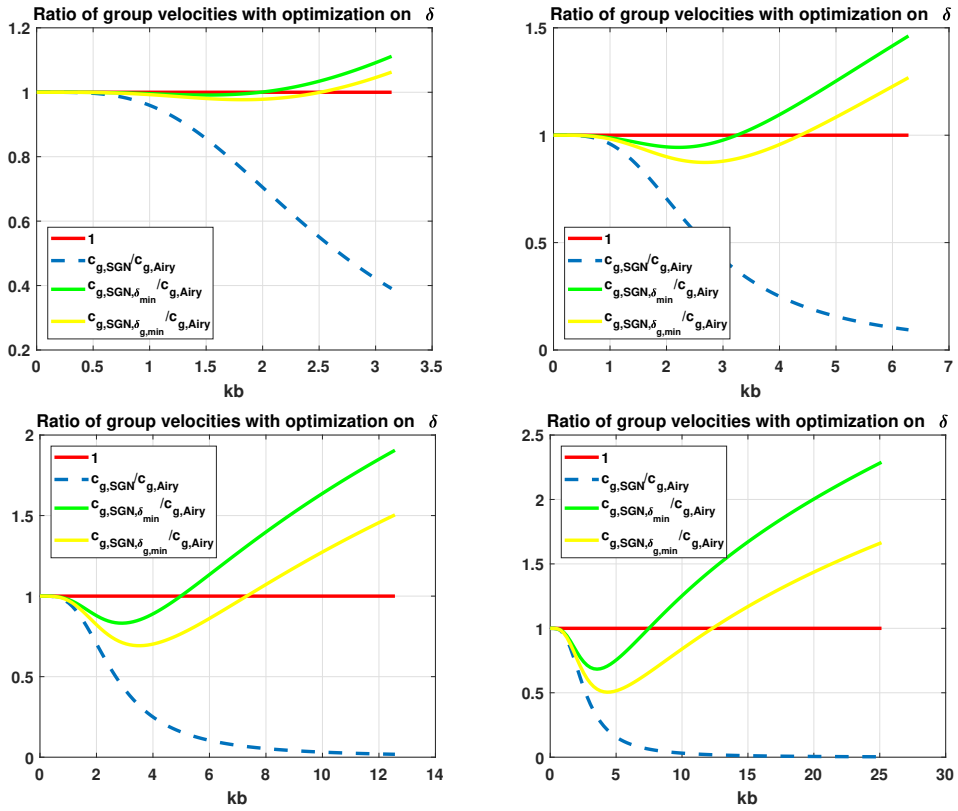

Figure 3: $c_{g,\mathrm{SGN},\delta_{\min}}/c_{g,\mathrm{Airy}}$ for several values of $x_{\max}$. Up left: $x_{\max} = \pi$, up right: $x_{\max} = 2\pi$, bottom left: $x_{\max} = 4\pi$, bottom right: $x_{\max} = 8\pi$. $N = 100$.

4. Numerical tests

In this Section, we first detail some elements of the numerical method used, in particular on the discretization of the elliptic equation. For further details on the discretization of the hyperbolic part of the SGN equations, we refer to a previous study from some of the authors, [34]. Next, a set of numerical tests has been selected to highlight the applicability of this new framework and the effects of the improved dispersion on the quality of the results both for linear and nonlinear problems. As we are interested here in nearshore wave propagation, we therefore consider, as is customary in coastal engineering, kb in $[0, \pi]$. Thus, in line with the results of Section 3.2, we take the value 0.17 for the dispersion correction parameter δ in the tests considered in Section 4.4 and 4.3.

4.1. Numerical method

A key point of the numerical method used in the present study is that it avoids splitting the free surface gradient into an artificial flux gradient and a source term, which accounts for bed slope. As a result, the free surface gradient is computed separately from the numerical flux, eliminating the need for additional treatments to guarantee the well-balanced properties of the scheme [34]. Note also that the mass and momentum equations are taken in conservative form, so that the system to be solved is

$$
\begin{aligned}
&\partial_t h + \partial_x (hv) = 0,\\
&\partial_t (hv) + \partial_x (hv^2) + gh\partial_x \eta = \partial_x \widetilde{p} - p_b \partial_x b,\\
&4(1+\delta)\partial_x \left(\frac{\partial_x \widetilde{p}}{hY} \right) - 6 \left[\frac{2}{h^3} \, \frac{Y-3}{Y} + \partial_x \left(\frac{\partial_x b}{h^2 Y} \right) \right] \widetilde{p}\\
&\qquad\qquad = \partial_x \left(g\partial_x \eta + \frac{R\partial_x b}{Y} \right) - 6\frac{R}{hY} + 2\left(\partial_x v\right)^2 .
\end{aligned}
\tag{21}
$$

In the sequel on this Subsection, we provide the hyperbolic solver first, next the elliptic solver, then the numerical scheme associated to the time-integration and finally we explain how the wave generation has been done.

4.1.1. Hyperbolic solver

The space discretization of the hyperbolic part of these equations - formally obtained for non-hydrostatic pressure components $\widetilde{p}$ and p_b going to zero - is based on an approach allowing momentum conservation on staggered grids [35]. This technique has been proven to be appropriate for rapidly varying flows, such as bores and inundation of dry land [34]. It is summarized here to make the present paper self-contained. The variables are approximated on a staggered grid: the total water depth h and the bed topography b are defined at the cell center i, and the depth-averaged velocity v is stored at the cell interfaces $i \pm 1/2$. The water depth h is evaluated at each time step level $t = n\Delta t$, whereas the depth-averaged velocity v is evaluated halfway between the present and the following time step, *i.e.* at $t = [n + (1/2)]\,\Delta t$. This leads to the staggering of spatial and temporal information and facilitates consistent second-order accuracy in space and time. The mass equation is discretized as

$$
\frac{h_i^{n+1} - h_i^n}{\Delta t} + \frac{1}{\Delta x} \left(\hat{h}_{i+1/2}^n v_{i+1/2}^{n+1/2} - \hat{h}_{i-1/2}^n v_{i-1/2}^{n+1/2} \right) \approx 0, \tag{22}
$$

where $\hat{h}_{i\pm1/2}$ are the water depths at the cell interfaces computed with an upwind approximation:

$$
\hat{h}_{i+1/2}^n \approx \begin{cases} h_i^n & \text{if } v_{i+1/2}^{n+1/2} \geq 0, \\ h_{i+1}^n & \text{if } v_{i+1/2}^{n+1/2} < 0. \end{cases} \tag{23}
$$

The next step is the solution of the momentum equation. For this, we employ the finite difference approximations recommended in Zijlema [35] to achieve conservation of the momentum flux across discontinuities, as

$$
\frac{\overline{h}_{i+1/2}^{n+1} v_{i+1/2}^{n+3/2} - \overline{h}_{i+1/2}^{n} v_{i+1/2}^{n+1/2}}{\Delta t} + \frac{\hat{v}_{i+1}^{n+1/2} \overline{q}_{i+1}^n - \hat{v}_i^{n+1/2} \overline{q}_i^n}{\Delta x} \approx -g\overline{h}_{i+1/2}^{n+1} \frac{\eta_{i+1}^{n+1} - \eta_i^{n+1}}{\Delta x}. \tag{24}
$$

Regarding the free surface gradient term, the use of the updated variable $\overline{h}_{i+1/2}^{n+1}$ is necessary for the scheme to guarantee the entropy inequality, as demonstrated in [36]. Further, it is necessary to approximate the convection term with an upwind scheme, where the mass flux q is the criterium for upwinding and the velocity v is the upwinded quantity:

$$\hat{v}_i^{n+1/2} \approx v_{i-1/2}^{n+1/2} \text{if } \overline{q}_i^n \geq 0, \qquad v_{i+1/2}^{n+1/2} \text{if } \overline{q}_i^n < 0. \tag{25}$$

It is important to note that a reversed approach where the upwinded quantity is q, leads to errors in the computation of the momentum fluxes across discontinuities, as demonstrated by Zijlema [35]. Also, since the mass flux q is continuous, an averaged approximation can be used for its computation, as

$$\overline{q}_{i+1/2}^n \approx \frac{1}{2}(q_i^n + q_{i+1}^n). \tag{26}$$

The flow depth, originally defined at the cell centroid, is also approximated at the cell interface with arithmetic averaging to be used in the computation of the local acceleration:

$$\overline{h}_{i+1/2}^{n+1} \approx \frac{1}{2}(h_i^{n+1} + h_{i+1}^{n+1}). \tag{27}$$

To counter numerical dissipation, the above-described first-order upwind scheme is extended to second-order accuracy by using the Minmod slope limiter [37].

4.1.2. Elliptic solver

The non-hydrostatic source terms are computed by solving the elliptic equation (21), which is discretized as

$$\int_{x_{i-\frac{1}{2}}}^{x_{i+\frac{1}{2}}} 4\,(1+\delta)\,\partial_x\left(\frac{\partial_x \widetilde{p}}{hY}\right)\,\mathrm{d}x \approx \left(\frac{K_{i+1}+K_i}{2\Delta x}\right)\widetilde{p}_{i+1} - \left(\frac{K_{i+1}+2K_i+K_{i-1}}{2\Delta x}\right)\widetilde{p}_i + \left(\frac{K_i+K_{i-1}}{2\Delta x}\right)\widetilde{p}_{i-1}, \tag{28}$$

where $K_i = 4(1+\delta)h_i^{-1}\left[4 + \dfrac{(b_{i+1}-b_{i-1})^2}{4(\Delta x)^2}\right]^{-1}$. The second term in the left-hand side of Equation (21) is discretized as

$$\int_{x_{i-\frac{1}{2}}}^{x_{i+\frac{1}{2}}} 6\left[\frac{2}{h^3}\frac{Y-3}{Y} + \partial_x\left(\frac{\partial_x b}{h^2 Y}\right)\right]\widetilde{p}\,\mathrm{d}x = 6\left[\frac{\Delta x}{h_i^3}\frac{Y_i-3}{Y_i} + \left(\frac{\partial_x b}{h^2 Y}\right)_{i+1/2} - \left(\frac{\partial_x b}{h^2 Y}\right)_{i-1/2}\right]\widetilde{p}_i. \tag{29}$$

The source term of Equation (21), denoted by F, is discretized as

$$F_i = \int_{x_{i-\frac{1}{2}}}^{x_{i+\frac{1}{2}}} \left\{\partial_x\left(g\partial_x\eta + \frac{R\partial_x b}{Y}\right) - 6\frac{R}{hY} + 2\left(\partial_x v\right)^2\right\}\mathrm{d}x \approx \left(g\partial_x\eta + \frac{R\partial_x b}{Y}\right)_{i+1/2} - \left(g\partial_x\eta + \frac{R\partial_x b}{Y}\right)_{i-1/2} - \Delta x\frac{6R_i}{h_i Y_i} + \frac{2\left(v_{i+1/2}-v_{i-1/2}\right)^2}{\Delta x},$$

where centered finite difference schemes are used for the discretization of the space derivatives of h and η. The following tridiagonal system is thus obtained :

$$\alpha_{i-1}\widetilde{p}_{i-1} + \alpha_i\widetilde{p}_i + \alpha_{i+1}\widetilde{p}_{i+1} \approx F_i, \tag{30}$$

where

$$\alpha_{i-1} = \frac{K_i + K_{i-1}}{2\Delta x}, \tag{31}$$

$$\alpha_i = -\frac{K_{i+1}+2K_i+K_{i-1}}{2\Delta x} - 6\left[\frac{1}{h_i^3}\frac{Y_i-3}{Y_i} + \left(\frac{\partial_x b}{h^2 Y}\right)_{i+1/2} - \left(\frac{\partial_x b}{h^2 Y}\right)_{i-1/2}\right], \tag{32}$$

$$\alpha_{i+1} = \frac{K_{i+1}+K_i}{2\Delta x}. \tag{33}$$

This system is solved with the Thomas algorithm, and the non-hydrostatic pressure at the bottom, p_b, is then calculated at a cell i by

$$p_{b\,i} \approx \frac{1}{Y_i}\left(\frac{6\widetilde{p}_i}{h_i} + h_i Y_i \frac{\widetilde{p}_{i+1} - \widetilde{p}_{i-1}}{2\Delta x}\ \frac{b_{i+1} - b_{i-1}}{2\Delta x}\right). \tag{34}$$

Finally, the non-hydrostatic terms are added to the momentum equation as

$$(\partial_x \widetilde{p} - p_b \partial_x b)_{i+1/2} \approx \frac{\widetilde{p}_{i+1} - \widetilde{p}_i}{\Delta x} + \frac{p_{b\,i+1} + p_{b\,i}}{2}\ \frac{b_{i+1} - b_i}{\Delta x}. \tag{35}$$

4.1.3. Time integration

To match the second-order accuracy in space, a combination of the Leapfrog scheme and the Runge-Kutta prediction-correction method [38] is used. The hyperbolic equations are written in vector form, with a splitting of the terms into local and convective accelerations, and pressure terms, as

$$\partial_t \boldsymbol{U} + \boldsymbol{F}(\boldsymbol{U}) + \boldsymbol{P}(\boldsymbol{U}) + \boldsymbol{Q}(\boldsymbol{U}) = \boldsymbol{0}, \tag{36}$$

where $\boldsymbol{U} = [h,\ hv]^{\mathrm{T}}$, and

$$\boldsymbol{F}(\boldsymbol{U}) = \begin{bmatrix} \partial_x(hv) \\ \partial_x(hv^2) \end{bmatrix}, \boldsymbol{P}(\boldsymbol{U}) = \begin{bmatrix} 0 \\ gh\partial_x \eta \end{bmatrix}, \boldsymbol{Q}(\boldsymbol{U}) = \begin{bmatrix} 0 \\ -\partial_x \widetilde{p} + p_b \partial_x b \end{bmatrix}. \tag{37}$$

The variable $\boldsymbol{U}$ is calculated using a two-stage time integration with an intermediate solution obtained by the prediction step. In the first step, the equations are solved with only the advection terms and the non-hydrostatic pressure on the right-hand side:

$$\boldsymbol{U}_i^* \approx \boldsymbol{U}_i^n - \Delta t \boldsymbol{F}(\boldsymbol{U}_i^n) - \Delta t \boldsymbol{Q}(\boldsymbol{U}_i^n). \tag{38}$$

In the second step, the hydrostatic pressure term is added to the momentum equations, and, to achieve second-order accuracy in time, the predicted variables are corrected by

$$\boldsymbol{U}_i^{n+1} \approx \frac{\Delta t}{2}(\boldsymbol{U}_i^n + \boldsymbol{U}_i^*) - \frac{\Delta t}{2}\boldsymbol{F}(\boldsymbol{U}_i^*) - \frac{\Delta t}{2}\boldsymbol{Q}(\boldsymbol{U}_i^*) - \Delta t \boldsymbol{P}\left(\boldsymbol{U}_i^{n+1}\right). \tag{39}$$

It is important to note that the surface gradient term $\boldsymbol{P}(\boldsymbol{U})$ must be excluded to the prediction step of the time integration. Second-order accuracy is achieved for the calculation of this term by employing the Leapfrog scheme in conjunction with staggering the variables in time.

The time stepping is limited by the Courant-Friedrichs-Levy (CFL) constraint and essentially depends on the cell size and the maximum speed of the gravity waves superposed to the motion of the fluid particles. Similar to other published SGN and Boussinesq-type numerical solutions (see *e.g.* [39, 40, 41, 1]), the time step is computed based on the condition:

$$\Delta t = \frac{\mathrm{CFL}\ \Delta x}{|v_{i+\frac{1}{2}}| + \sqrt{g h_{i+\frac{1}{2}}}}. \tag{40}$$

In the following numerical experiments, the CFL number is taken as 0.5 since it is enough to get a stable numerical scheme .

4.1.4. Wave generation

The numerical implementation of the wave generation is based on the internal wavemaker approach proposed by [42]. A source term is introduced in the continuity equation, with the effect of adding and subtracting mass. Since in the original method the source term was derived for the equation by Nwogu [33], the source term had to be adapted to satisfy the present governing equation. For a monochromatic wave

of amplitude a, wave number k, and angular frequency ω, the magnitude of the source function has been modified to account for the free parameter δ in the dispersion relation, as

$$D = \frac{2a\left[\omega^2 + \frac{1}{3}\delta g k^4 h^3\right]}{\omega k I_1\left[1 + \frac{1}{3}\left(1+\delta\right)k^2h^2\right]}, \tag{41}$$

where I_1 is a function of the wavenumber (see [42] for details). The wave absorption at the boundaries is then achieved through the sponge layer technique described in [43].

4.2. Sine wave propagation in constant depth

In this section, we test the applicability and stability of the modified SGN equations in a numerical framework. The first test is the propagation of linear monochromatic waves in a long channel of constant depth. Inside the one-dimensional computational domain, we generate and propagate linear waves ($\epsilon = \eta_0/b_0 = 0.01 \ll 1$) with varying wavelengths, resulting in different shallowness parameters (*i.e.*, $kb_0 = 1, 3, 5,$ and 10). To achieve the exact dispersion properties, the dispersion correction parameter $\delta = \delta_0$ is determined for each value of kb_0 by Equation (20). Several numerical tests with different grid resolutions and time steps show that the solution has converged with $\mathrm{CFL} = 0.5$ and a grid size Δx such that the number of grid points per wavelength is $\lambda_0/\Delta x = 20$. The numerical results reveal no significant change with additional refinement. With a coarse grid (*i.e.* $\lambda_0/\Delta x = 15$), we notice a small dispersive error, which leads to a shorter wavelength than the exact solution described by Airy wave theory.

The results of the proposed modified SGN model are shown in Figure 4, and can be compared to the fully dispersive Airy wave theory. With a suitable value of the parameter δ, the proposed model is stable even at high values of kb_0 and accurately reproduces the monochromatic wave propagation in terms of shape and speed. Note that numerical results with the original SGN equations (*i.e.* with $\delta = 0$) are not shown in Figure 4. The numerical solutions without dispersion correction are unstable due to the excessive dispersion error and thus do not converge.

4.3. Periodic wave propagation over a submerged bar

We now consider the test of periodic wave propagation over a submerged bar. The numerical results are compared with experimental measurements obtained by Beji and Battjes [44]. Figure 5 (a) depicts the laboratory setup, which includes a $37.7\,\mathrm{m}$ long and $0.75\,\mathrm{m}$ tall flume with a $0.30\,\mathrm{m}$ tall trapezoidal bar $6\,\mathrm{m}$ away from a piston-type wavemaker. The front slope of the bar is 1:20, followed by a 2-meter crest and a 1:10 rear slope. At the end of the flume, a gravel beach is installed, which functions as a wave absorber. For the simulations, we use the computational domain shown in Figure 5 (b). Waves shoal when propagating up the slope of the bar. This produces a cascade of several bound higher harmonics each with less energy than the previous. While these waves are not very dispersive on top of the bar due to the relatively shallow water depth, their kh-value rapidly increases at the lee side where the relative water depth increases rapidly.

We use the experimental data from case A of [44], which involves a sinusoidal wave with a $1\,\mathrm{cm}$ amplitude and $2.02\,\mathrm{s}$ period. The test was conducted in $0.4\,\mathrm{m}$ water depth, resulting in a $kb_0 = 0.67$ incident wave. The numerical tests have been run using a $\Delta x = 0.02\,\mathrm{m}$ grid size, and $\mathrm{CFL} = 0.5$.

The wave generation works in the same way as in the previous test from Section (4.2). While the incident wave is fairly long and can be well resolved with the original SGN equations, the super-harmonics behind the bar require high-order dispersion properties to be adequately computed. We test both the original SGN equations (*i.e.*, $\delta = 0$) and the modified SGN equations with $\delta = 0.17$, which corresponds to the value -0.39 for α in the Nwogu system, as recommended in [33]. Note that this is equivalent to the choice of $x_{\max} = (kb)_{\max} = \pi$ (see Table 1).

The recorded time series at different wave gauges showcase the difference between the two sets of equations; see Figure 6. Both the original and modified SGN equations maintain good agreement with experimental data at stations 4, 5, and 6 over the bar, proving the quality of numerical solutions regarding wave propagation and shoaling. The solutions of the two models significantly diverge behind the bar at stations 8–11, where super-harmonics of high kb-values are present. While the modified SGN model is able to capture the overall wavefield behind the bar with only minor discrepancies, the original SGN model fails at computing the released short waves due to the poor dispersive properties of the governing equations. This test case clearly showcases the impact of high-dispersive errors on the accuracy and stability of the solution. The modified SGN model, with its enhanced dispersion, achieves improved accuracy, especially for the gauges behind the bar.

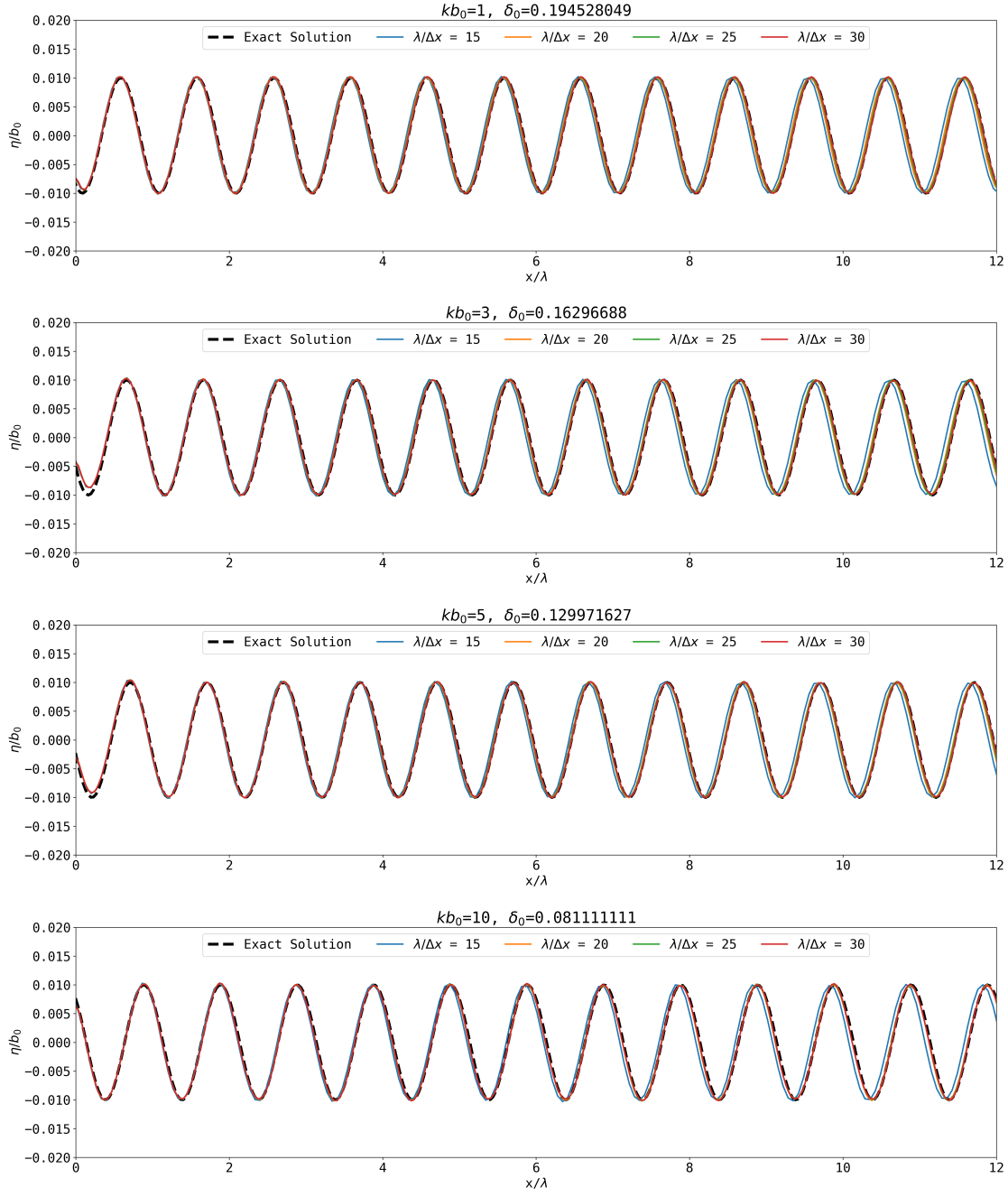

Figure 4: Sine wave on flat bottom; *cf.* Section 4.2. The black line, which represents the analytical solution from Airy wave theory, and the colored lines represent the numerical solutions of the modified SGN equations at different grid resolutions.

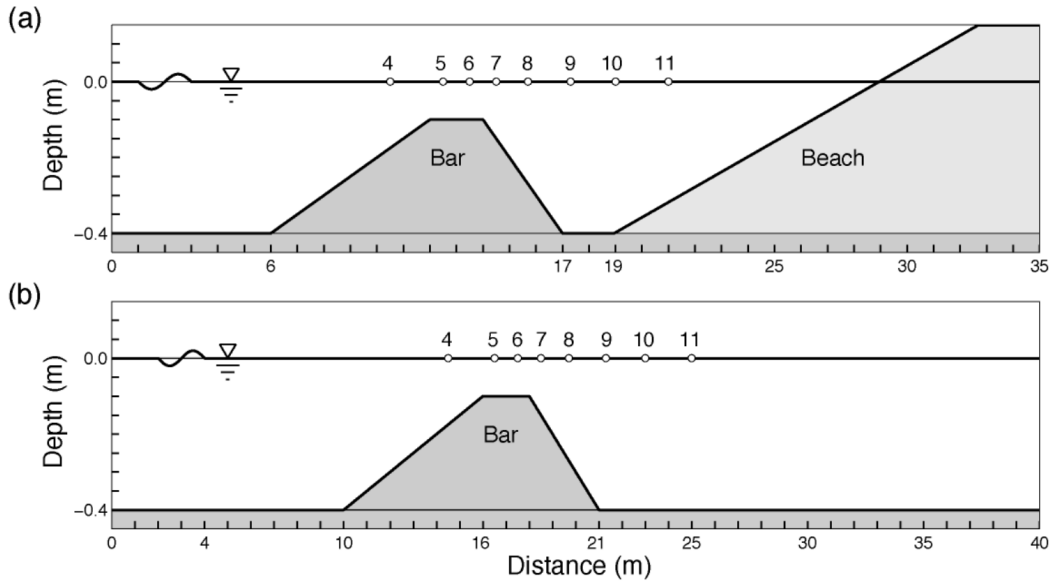

Figure 5: Periodic wave propagation over a submerged bar; *cf.* Section 4.3. (a) Laboratory setup from Reference [44]. (b) Numerical model setup. Circles indicate gauge locations. Figure adapted from [45].

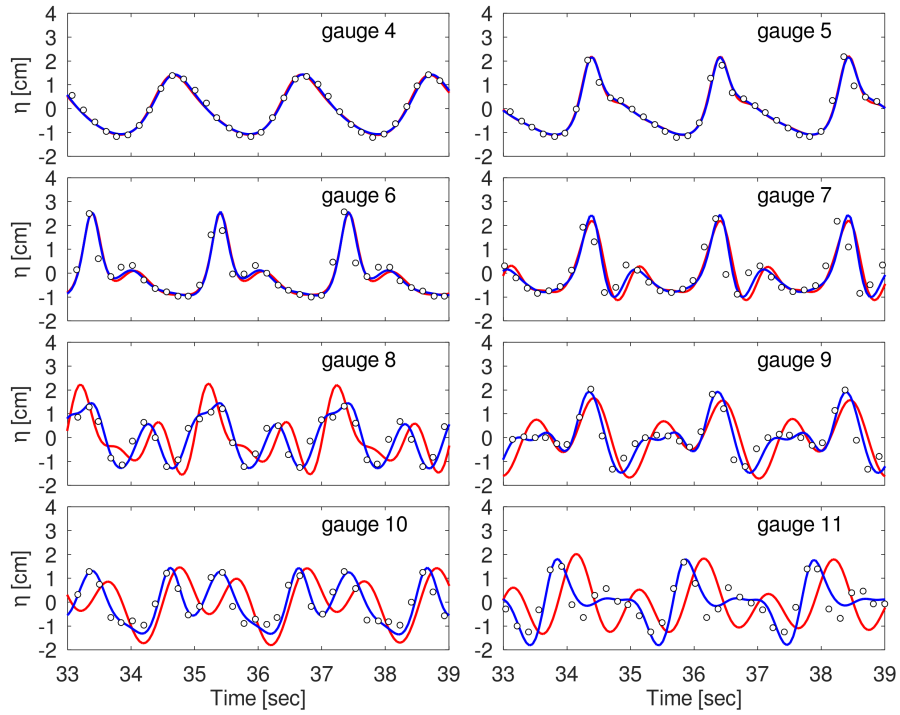

Figure 6: Periodic wave propagation over a submerged bar; *cf.* Section 4.3. Circles indicate laboratory data from Reference [44]. The red lines are time series from the solution of the original SGN model and the blue lines represent the results of the modified SGN equations.

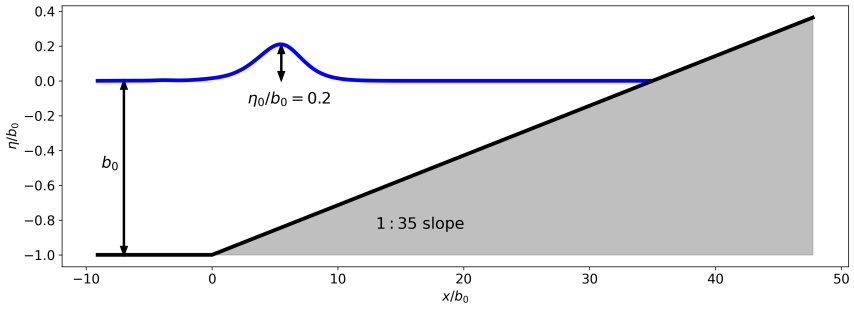

Figure 7: Non-linear shoaling of a solitary wave on a plane beach; *cf.* Section 4.4. Numerical model setup.

4.4. Nonlinear shoaling of a solitary wave over a plane beach

Finally, we consider the test presented in [46], of a solitary wave shoaling over a plane slope. The test consists of a solitary wave with amplitude $a = 0.088\,\mathrm{m}$ propagating in a $b_0 = 0.44\,\mathrm{m}$ water depth, *i.e.* $a/b_0 = 0.2$, and shoaling over a constant slope $1 : 35$. It is worth noting that during the test, the local values of the non-linearity parameter ε prior to breaking are between 0.2 and 2.2, and thus the benchmark is suitable for testing the nonlinear properties of the equations.

The computational domain of the test is shown in Figure 7. The coordinates were set so that the slope's toe corresponds to $x = 0$. The generation of the solitary wave is achieved through the leftward boundary condition and follows the standard solitary wave profile given below:

$$\eta\left(x,t\right) = a\,\mathrm{sech}^2\left(\sqrt{\frac{3a}{4b_0^3}}\left[x - x_0 - t\sqrt{g\left(a+b_0\right)}\right]\right),$$

$$v\left(x,t\right) = \frac{\eta\left(x,t\right)}{b_0+\eta\left(x,t\right)}\sqrt{g\left(a+b_0\right)}.$$

The numerical solutions of both the original and modified SGN equations are compared with laboratory data given in Reference [46]. During the experiment, the free surface elevation was recorded at nine gauges on the slope. The last gauge (*i.e.* G9) is located close to the wave breaking point. The numerical results are fully converged for the grid size $\Delta x = 0.005\,\mathrm{m}$ and the CFL number of 0.5. Similar to the previous test, we take $\delta = 0.17$.

The results are shown in Figure 8. The results obtained with the modified SGN equations show a better overall match with the laboratory data compared to the original equations, which are composed of weaker dispersion properties. While the modified SGN equation well captures the shape, height, and speed of the shoaling wave, the original equation, with its low dispersion properties, underestimates the wave height and the speed of the wave. We find that the proposed modification of the elliptic equations leads to improved shoaling properties in the nonlinear regimes. While the optimization of the free parameter was based on the linear dispersion relationship of the equation, the improved formulation still holds for nonlinear processes such as shoaling.

5. Conclusion

A method for dispersion correction of the weakly dispersive Serre-Green-Naghdi equations is presented along with its detailed justification. The proposed modification of the equations relies on a form of the model where an elliptic equation fulfilled by the depth-integrated non-hydrostatic pressure is solved coupled with the mass and momentum equations. It is simple to implement in the sense that it does not require the inclusion of new terms with high-order derivatives into the equations of the original model. The insertion of the dispersion correction parameter in the equations results in introducing terms of $O(\sigma^4)$ in the elliptic equation. This can be advantageous compared to classical dispersion correction methods, for which the added terms are of $O(\sigma^5)$ baring potential problems for the numerical instability, or in $O(\sigma^3)$, then of the same order as the dispersive terms present in the original equations.

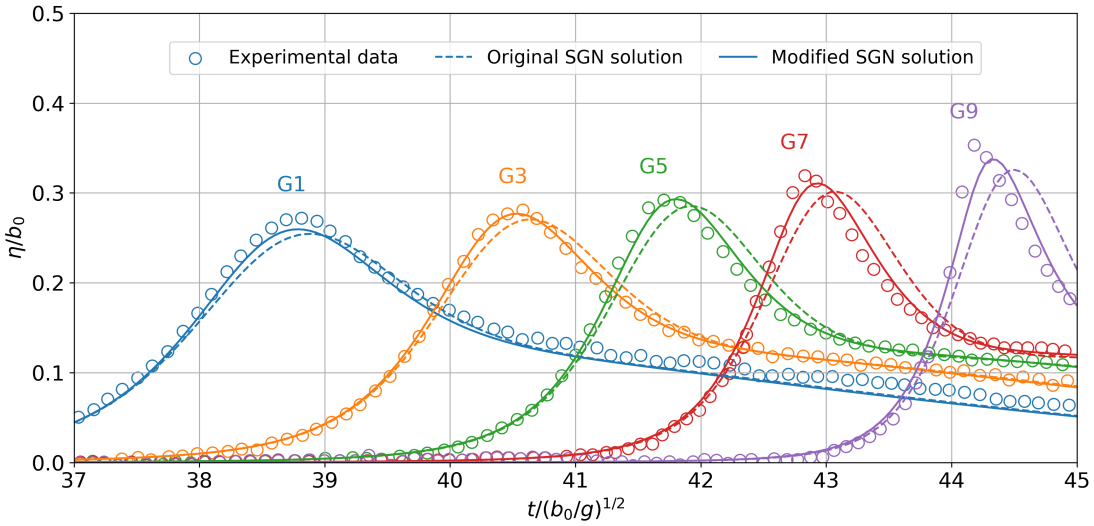

Figure 8: Non-linear shoaling of a solitary wave on a plane beach; *cf.* Section 4.4. Comparison between computed wave heights at gauges 1, 3, 5, 7 and data from Reference [46].

Relevant one-dimensional tests confirm the efficiency of the proposed dispersion correction in an almost linear regime, in regimes where both non-linearity and dispersion increase, and in a fully non-linear regime. The results obtained for the tests with bathymetry variable in space are encouraging, even if the method was not specifically designed for such a setting.

Competing Interests

The authors declare no conflict of interest. The funding agencies had no role in the design of the study; in analyses or interpretation of data; in the writing of the manuscript; or in the decision to publish the results.

Data availability

The routines for replication of the numerical results can be provided upon reasonable request.

Acknowledgements

The authors are listed in alphabetical order. We acknowledge financial support from the I-SITE program Energy & Environment Solutions (E2S), the Communauté d'Agglomération Pays Basque (CAPB), and the Communauté Région Nouvelle Aquitaine (CRNA) for the chair position HPC-Waves and for supporting the Kostarisk Laboratoire Commun. We also acknowledge support from the European Union's Horizon 2020 research and innovation program under grant agreement No 883553.

References

[1] V. Roeber and K. F. Cheung. Boussinesq-type model for energetic breaking waves in fringing reef environments. *Coast. Eng.*, 70:1–20, 2012.

[2] J. T. Kirby. Recent advances in nearshore wave, circulation, and sediment transport modeling. *J. Mar. Res.*, 75:263–300, 2017.

[3] J. S. Antunes do Carmo, J. A. Ferreira, and L. Pinto. On the accurate simulation of nearshore and dam break problems involving dispersive breaking waves. *Wave Motion*, 85:125–143, 2019.

[4] O. B. Fringer, C. N. Dawson, R. He, D. K. Ralston, and Y. J. Zhang. The future of coastal and estuarine modeling: Findings from a workshop. *Ocean Model.*, 143:101458, 2019.

[5] A. G. Filippini, S. Bellec, M. Colin, and M. Ricchiuto. On the nonlinear behaviour of Boussinesq type models: Amplitude-velocity vs amplitude-flux forms. *Coast. Eng.*, 99:109–123, 2015.

[6] G. Khakimzyanov, D. Dutykh, Z. Fedotova, and D. Mitsotakis. Dispersive shallow water wave modelling. Part I : Model derivation on a globally flat space. *Commun. Comput. Phys.*, 23:1–29, 2018.

[7] D. Lannes. Modeling shallow water waves. *Nonlinearity*, 33:R1, 2020.

[8] F. Serre. Contribution à l'étude des écoulements permanents et variables dans les canaux. *La Houille Blanche*, 3:374–388, 1953.

[9] C. H. Su and C. S. Gardner. Korteweg-de Vries equation and generalizations. III. Derivation of the Korteweg-de Vries equation and Burgers equation. *J. Math. Phys.*, 10:536–539, 1969.

[10] A. E. Green and P. M. Naghdi. A derivation of equations for wave propagation in water of variable depth. *J. Fluid Mech.*, 78:237–246, 1976.

[11] T. B. Benjamin, J. L. Bona, and J. J. Mahony. Model equations for long waves in nonlinear dispersive systems. *Philos. Trans. Royal Soc. A*, 272:47–78, 1972.

[12] P. A. Madsen, H. B. Bingham, and H. A. Schäffer. Boussinesq-type formulations for fully nonlinear and extremely dispersive water waves: derivation and analysis. *Proc. R. Soc. Lond. A*, 459:1075–1104, 2003.

[13] J. M. Witting. A unified model for the evolution of nonlinear water waves. *J. Comput. Phys.*, 56:203–236, 1984.

[14] A. Schröter, R. Mayerle, and W. Zielke. Optimized dispersion characteristics of the Boussinesq wave equations. In *Proc. Waves - Physical and numerical modelling*, pages 416–425, Vancouver, Canada, 1994.

[15] P. A. Madsen, R. Murray, and O. R. Sørensen. A new form of the Boussinesq equations with improved linear dispersion characteristics. *Coast. Eng.*, 15:371–388, 1991.

[16] P. A. Madsen and O. R. Sørensen. A new form of the Boussinesq equations with improved linear dispersion characteristics. Part 2. A slowly-varying bathymetry. *Coast. Eng.*, 18:183–204, 1992.

[17] P. A. Madsen and H. A. Schäffer. Higher-order Boussinesq-type equations for surface gravity waves: derivation and analysis. *Philos. Trans. Royal Soc. A*, 356:3123–3184, 1998.

[18] C. H. Cienfuegos, E. Barthélemy, and P. Bonneton. A fourth-order compact finite volume scheme for fully nonlinear and weakly dispersive Boussinesq-type equations. Part I: Model development and analysis. *Int. J. Numer. Methods Fluids*, 51:1217–1253, 2006.

[19] Z. B. Liu and Z. C. Sun. Two sets of higher-order Boussinesq-type equations for water waves. *Ocean Model.*, 32:1296–1310, 2005.

[20] F. Dias and P. Milewski. On the fully-nonlinear shallow-water generalized Serre equations. *Phys. Lett. A*, 99:1049–1053, 2010.

[21] J. S. Antunes do Carmo. Boussinesq and Serre type models with improved linear dispersion characteristics: Applications. *J. Hydraul. Res.*, 51:719–727, 2013.

[22] D. Clamond, D. Dutykh, and D. Mitsotakis. Conservative modified Serre–Green–Naghdi equations with improved dispersion characteristics. *Commun. Nonlinear Sci. Numer. Simulat.*, 45:245–257, 2017.

[23] P. Bonneton, F. Chazel, D. Lannes, F. Marche, and M. Tissier. A splitting approach for the fully nonlinear and weakly dispersive Green-Naghdi model. *J. Comput. Phys.*, 230:1479–1498, 2011.

[24] F. Chazel, D. Lannes, and F. Marche. Numerical simulation of strongly nonlinear and dispersive waves using a Green–Naghdi model. *J. Sci. Comput*, 48:105–116, 2011.

[25] A. G. Filippini, M. Kazolea, and M. Ricchiuto. A flexible genuinely nonlinear approach for nonlinear wave propagation, breaking and run-up. *J. Comput. Phys.*, 230:381–417, 2016.

[26] B. Alvarez-Samaniego and D. Lannes. Large time existence for 3D water-waves and asymptotics. *Invent. Math.*, 171:485–541, 2008.

[27] R. Chassagne, A. G. Filippini, M. Ricchiuto, and P. Bonneton. Dispersive and dispersive-like bores in channels with sloping banks. *J. Fluid Mech.*, 870:595–616, 2019.

[28] A. Cauquis, M. Ricchiuto, and P. Heinrich. Lax-Wendroff schemes with polynomial extrapolation and simplified Lax-Wendroff schemes for dispersive waves: a comparative study. *Water Waves*, 4:345–377, 2022.

[29] G. Khakimzyanov, D. Dutykh, O. Gusev, and N. Shokina. Dispersive shallow water wave modelling. Part II : Numerical simulation on a globally flat space. *Commun. Comput. Phys.*, 23:30–92, 2018.

[30] J. Miles and R. Salmon. Weakly dispersive nonlinear gravity waves. *J. Fluid Mech.*, 157:519–531, 1985.

[31] D. Clamond. Remarks on dispersion-improved shallow water equations with uneven bottom. *J. Phys. A: Math. Theor.*, 54:045701, 2021.

[32] F. J. Seabra-Santos, D. P. Renouard, and A. M. Temperville. Numerical and experimental study of the transformation of a solitary wave over a shelf or isolated obstacle. *J. Fluid Mech.*, 176:117–134, 1987.

[33] O. Nwogu. Alternative form of Boussinesq equations for nearshore wave propagation. *J. Waterw. Port Coast. Ocean Eng.*, 119:618–638, 1993.

[34] F.-Z. Mihami, V. Roeber, and D. Morichon. Efficient numerical computations of long-wave run-up and their sensitivity to grid nesting. *Water Waves*, 17:517–548, 2022.

[35] M. Zijlema. The role of the Rankine-Hugoniot relations in staggered finite difference schemes for the shallow water equations. *Comput. Fluids*, 192:104274, 2019.

[36] D. Doyen and P. H. Gunawan. An explicit staggered finite volume scheme for the shallow water equations. In *Finite Volumes for Complex Applications VII-Methods and Theoretical Aspects*, pages 227–235. Springer, 2014.

[37] F. Moukalled, L. Mangani, and M. Darwish. *The finite volume method in computational fluid dynamics*. Springer International Publishing, Switzerland, 2011.

[38] S. Gottlieb and C.-W. Shu. Total variation diminishing Runge-Kutta schemes. *Math. Comput.*, 67:73–85, 1998.

[39] N. Favrie and S. Gavrilyuk. A rapid numerical method for solving Serre–Green–Naghdi equations describing long free surface gravity waves. *Nonlinearity*, 30:2718, 2017.

[40] M Kazolea and A. I. Delis. A well-balanced shock-capturing hybrid finite volume–finite difference numerical scheme for extended 1D Boussinesq models. *Appl. Numer. Math.*, 67:167–186, 2013.

[41] F. Shi, J. T. Kirby, J. C. Harris, J. D. Geiman, and S. T. Grilli. A high-order adaptive time-stepping TVD solver for Boussinesq modeling of breaking waves and coastal inundation. *Ocean Model.*, 43:36–51, 2012.

[42] G. Wei, J. T. Kirby, and A. Sinha. Generation of waves in Boussinesq models using a source function method. *Coast. Eng.*, 36:271–299, 1999.

[43] J. Larsen and H. Dancy. Open boundaries in short wave simulations—a new approach. *Coast. Eng.*, 7:285–297, 1983.

[44] S. Beji and J. A. Battjes. Experimental investigation of wave propagation over a bar. *Coast. Eng.*, 19:151–162, 1993.

[45] V. Roeber, K. F. Cheung, and M. H. Kobayashi. Shock-capturing Boussinesq-type model for nearshore wave processes. *Coast. Eng.*, 57:407–423, 2010.

[46] S. T. Grilli, R. Subramanya, I. A. Svendsen, and J. Veeramony. Shoaling of solitary waves on plane beaches. *J. Waterw. Port Coast. Ocean Eng.*, 120:609–628, 1994.